

The three-dimensional topological Dirac semimetal Na_3Bi : the ground state phase

Xiyue Cheng, Ronghan Li, Xing-Qiu Chen,* Dianzhong Li, and Yiyi Li
 Shenyang National Laboratory for Materials Science, Institute of Metal Research,
 Chinese Academy of Sciences, Shenyang 110016, China
 (Dated: June 15, 2021)

By means of first-principles calculations, we found that the early characterized three-dimensional topological bulk Dirac semimetal of the $P6_3/mmc$ Na_3Bi is dynamically unstable at the ground state due to the presence of the large imaginary phonon frequencies around the K point. Alternatively, our calculations suggest a new ground state phase which crystalizes in the $P\bar{3}c1$ structure with a buckled graphite-like Na/Bi sheets, which is both energetically and dynamically more stable. Moreover, the calculations also uncovered that the $P\bar{3}c1$ phase at the ground state is also a topological 3D Dirac semimetal, being exactly the same as the electronic states of the metastable $P6_3/mmc$ phase.

PACS numbers: 73.20.-r, 71.20.-b, 73.43.-f

Three-dimensional (3D) topological bulk Dirac semimetals (TDSs), as a new class of topological electronic state, is highlighting an exciting frontier of the Dirac electrons. In the TDSs, the conduction and valence bands touch only at the discrete Dirac points and disperse linearly in all directions in the Brillouin zone (BZ). This electronic state is different from the two-dimensional (2D) Dirac fermions in graphene and the surface state of the 3D topological insulators¹⁻⁴. The TDSs exhibits many attractive phenomena, on the one hand, in analog of graphene⁵, such as high electron mobility and conductivity in the 3D form, etc, and on the other hand, with numerous fascinating quantum properties, including the unique surface states in form of Fermi arcs, the Weyl phases, the high temperature linear quantum magnetoresistance and the topological magnetic phases as well as the anomalous Hall effect^{1-4,6-15}. In general, the TDSs are predicted to exist at the critical phase transition point from a normal insulator and a topological one through the spin-orbital coupling effect or by tuning the chemical composition^{9,16}. However, such bulk Dirac points are accidental degeneracies. Interestingly, very recently the systems of the $P6_3/mmc$ - Na_3Bi ¹⁻³ that one of the current authors participated in discovering¹ and β - BiO_2 ⁴ and Cd_3As_2 ^{10,17,18} have been demonstrated theoretically and then confirmed experimentally to be TDSs in their native phases as their 3D bulk Dirac fermions are indeed protected only by the crystallographic symmetry.

In particular, it has been noted that the crystal structure of the topological 3D bulk Dirac semimetal of Na_3Bi crystalizes in the Na_3As -type phase¹⁻³ with the space group of $P6_3/mmc$ and $Z=2$ which was firstly derived in 1937 by Brauer and Zintl¹⁹ from a Deby-Scherrer pattern, as shown in Fig. 1(a). However, as a matter of fact, the structure of the prototype compound Na_3As was re-investigated to correspond to other two closely correlated structures: the anti- LaF_3 -type (space group of $P\bar{3}c1$, $Z=6$, Fig. 1(d)) and the Cu_3P -type (space group $P6_3cm$, $Z=6$, Fig. 1(g)) revealed by Mansmann²⁰ and Hafner *et al.*^{21,22}, respectively. The experiments further uncovered that the $P6_3cm$ type structure was favored in the alkali-metal pnictides or nitrides and some intermetallic phases²³⁻²⁵, such as K_3Bi ²⁶, Cs_3As ²⁷, Mg_3Pt and Mg_3Cu ²⁸, while the $P\bar{3}c1$ phase is preferred in the trifluorides of the lanthanum group elements²⁹. Interestingly, because these two

TABLE I: Calculated equilibrium lattice constants of a (Å) and c (Å), the difference in total energy ΔE (meV/f.u.) and the optimized atomic sites for the $P6_3/mmc$, $P6_3cm$ and $P\bar{3}c1$ phases of Na_3Bi .

	a	c	ΔE	Atomic sites			
				Atom	x	y	z
$P6_3/mmc$	5.4579	9.7043	4.074	Na1	0	0	0.25
	5.448 ^a	9.655 ^a		Na2	0.3333	0.6667	0.5827
	5.459 ^b	9.674 ^b		Bi	0.3333	0.6667	0.25
$P\bar{3}c1$	9.4586	9.6740	0	Na1	0	0	0.25
	9.436 ^c	9.655 ^c		Na2	0.3333	0.6667	0.2003
				Na3	0.3542	0.3187	0.0833
				Bi	0.3368	0	0.25
$P6_3cm$	9.4559	9.6777	0.474	Na1	0	0	0.9809
				Na2	0.3333	0.6667	0.0582
				Na3	0.6970	0	0.1972
				Na4	0.3585	0	0.3637
				Bi	0.3309	0	0.0303

^a Reference², ^b Reference¹⁹ and ^c Reference²⁰.

structures are so close to each other that their X-Ray diffraction (XRD) patterns are almost indistinguishable for a specified compound^{28,29}.

Within the context, it is an urgent task to clarify the ground state phase of Na_3Bi . According to the Pearson's Handbook³⁰, Na_3Bi was attributed to the earlier characterized metastable $P6_3/mmc$ structure and the later studies focusing on Na_3Bi ^{1,2,31-38} all follow this structure. Here, by means of first-principles calculations, we have systematically investigated the phase stabilities and the electronic structures of Na_3Bi at the ground state. Our calculated results uncovered that the $P\bar{3}c1$ structure is the energetically favorable ground-state phase with thermodynamic and dynamical stabilities. However, the early characterized $P6_3/mmc$ structure is dynamically unstable with some large imaginary transverse acoustic (TA) modes around the high-symmetry K point at ground state. Importantly, their electronic band structures are similar to each other, featured by two 3D bulk Dirac fermions protected by the threefold rotated crystal symmetry. Therefore, our calculated results suggest that the ground state $P\bar{3}c1$ phase of Na_3Bi is also a robust TDS.

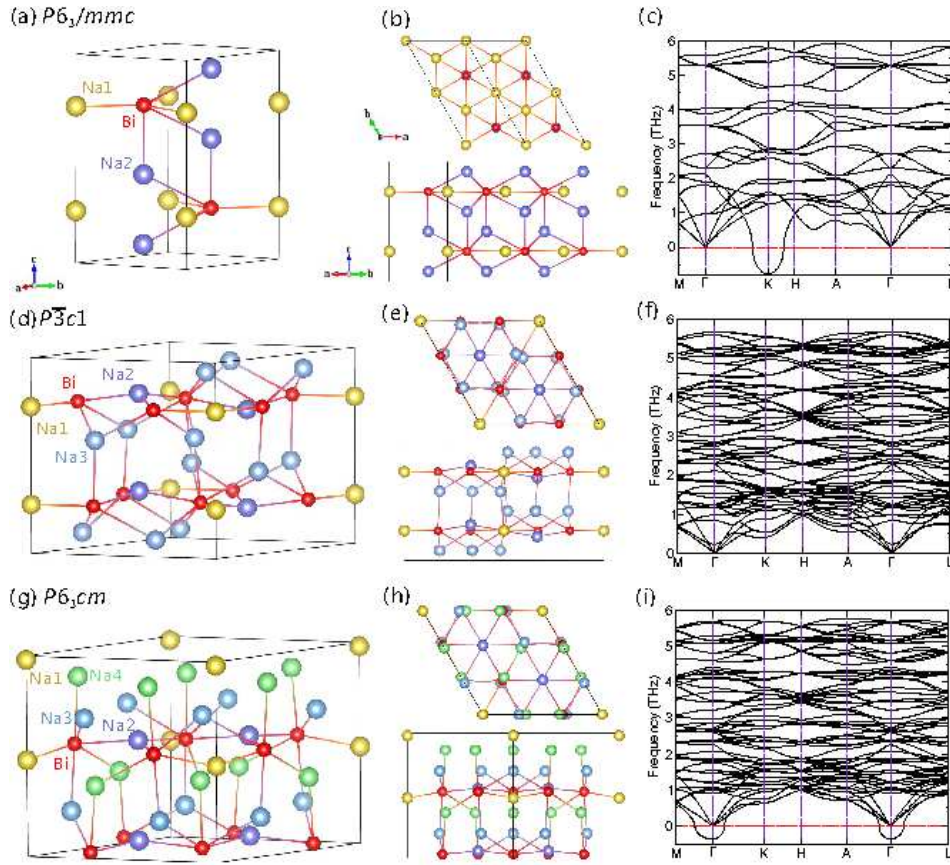


FIG. 1: Structure representations of (a) the original $P6_3/mmc$ (Na_3As -type) structure, (d) the $\overline{P3c1}$ (anti- LaF_3 -type) and (g) the $P6_3cm$ (Cu_3P -type) structures of Na_3Bi . The projection along the c axis and $[11\overline{2}0]$ directions for these three structures are shown in (b, e and h), together with the phonon dispersions in (c, f and i), respectively. Note that a $2\times 2\times 1$ supercell for $P6_3/mmc$ - Na_3Bi is used in the projection image (b). It needs to be emphasized that for these three structures Bi share the exactly same network, but the Na atoms distort highly ($P6_3/mmc$: two inequivalent Na atoms in (a); $\overline{P3c1}$: three inequivalent Na atoms in (d); $P6_3cm$: four inequivalent Na atoms in (g)).

The structural optimization and electronic properties of Na_3Bi were calculated within the framework of density functional theory (DFT)^{39,40} by employing the Vienna *ab initio* simulation package (VASP)^{41,42} with the projector augmented wave (PAW) method⁴³ and generalized gradient approximation (GGA) within the Perdew-Burke-Ernzerhof (PBE) exchange-correlation functional⁴⁴. The energy cutoff was set at 350 eV and appropriate Monkhorst-Pack k -meshes were chosen. A very accurate optimization of structural parameters was achieved by minimizing forces (below 0.0001 eV/Å) and stress tensors (typically below 0.5 k_B). To check the dynamical stability, we further derived the phonon dispersions using the finite-displacement approach as implemented in the *Phonopy* code⁴⁵.

The relative phase stabilities of three structures ($P6_3/mmc$, $\overline{P3c1}$ and $P6_3cm$) considered here for Na_3Bi can be visualized from the energy-vs-volume curves in Fig. 2. The $\overline{P3c1}$ - Na_3Bi is about 4 meV/f.u. lower in energy than the $P6_3/mmc$ structure. This small energy difference suggests that the metastable feature of the $P6_3/mmc$ structure which can be stable above about 46 K simply estimated according to $\Delta E = k_B T$. Interestingly, it has been noted that the $P6_3cm$ phase is energetically

comparable with the $\overline{P3c1}$ structure. Table I further compiles the optimized lattice parameters. Note that, as early as 1965 Mansmann suspected that Na_3Bi crystallizes in the $\overline{P3c1}$ structure and refined its lattice constants²⁰ in good agreement with our currently derived data in Table I, but he did not report the specified atomic sites.

The $P6_3/mmc$ phase has two formula units per unit cell ($Z = 2$), which is about one third in size of the other two competing structures ($Z = 6$). For the $P6_3/mmc$ phase, the Bi atom lies at $2c$ site ($1/3, 2/3, 1/4$) and the Na atoms occupy two inequivalent sites, Na1 at $2b$ site ($0, 0, 1/4$) and Na2 at $4f$ site ($1/3, 2/3, 0.58269$). This situation leads to a layered structure with the stacking sequence of Na-(graphite-like Na/Bi sheet)-Na and the graphite-like Na/Bi sheet is separated by the sodium atoms, as illustrated in Fig. 1(a, b). The Na-Bi distances within the graphite-like layers are around 3.151 Å and the vertical Na-Bi bonds between the adjacent layers are about 3.228 Å thus the Na and Bi atoms forming a base-centred tetrahedron.

In particular, the $P6_3/mmc$ structure is closely correlated with the $\overline{P3c1}$ one. The important difference is that in the $\overline{P3c1}$ structure the layered graphite-like Na/Bi sheets are distorted (Fig. 1(c and d)). At first, the upper/lower shifting

(about 0.05 Å) of the partial Na1 atoms along the c -axis in the $P6_3/mmc$ phase can be visualized, forming buckled graphite-like Na/Bi sheets. Secondly, the original Na2 atoms in the $P6_3/mmc$ phase distort within the ab -plane. Therefore, there are three inequivalent Na Wykoff sites in the $P\bar{3}c1$ structure (see Table I and Fig. 1d). Meanwhile, the bismuth atom is surrounded by seven Na atoms at the Na-Bi interacting distances ranging from 3.176 to 3.495 Å in the $P\bar{3}c1$ phase, whereas the coordination numbers for bismuth in the $P6_3/mmc$ structure is ten from the Na-Bi interacting distances from 3.152 to 3.544 Å.

Meanwhile, the $P6_3cm$ structure share a similar feature of this $P\bar{3}c1$ phase with buckled graphite-like Na/Bi sheets. But, their differences are also highly obvious. In the $P\bar{3}c1$ structure, the Na1 and Bi atoms lie in the same layer and the Na2 atoms are out of the the plane comprised by Na1 and Bi. However, in the $P6_3cm$ structure, the Na1 atom does not lie in the same layer as Bi stays (Fig. 1g). This difference can be clearly visualized from their projections along both $[0001]$ and $[11\bar{2}0]$ directions (Fig. 1(e and h)). It needs to be emphasized that K_3Bi was experimentally suggested to crystallize in this $P6_3cm$ structure²⁶. A complete description of that structure can be referred to Olofsson's detailed discussion²⁵.

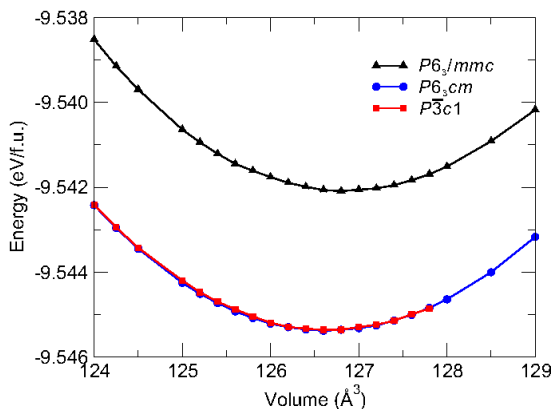


FIG. 2: The energy-versus volume curves for the $P6_3/mmc$, $P6_3cm$ and $P\bar{3}c1$ structure.

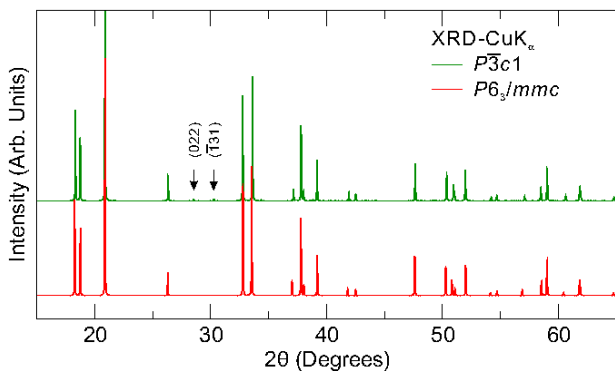


FIG. 3: The simulated XRD patterns (using Cu K_α radiation with $\lambda = 1.54439$ Å) for the $P\bar{3}c1$ (green) and $P6_3/mmc$ (red) structure.

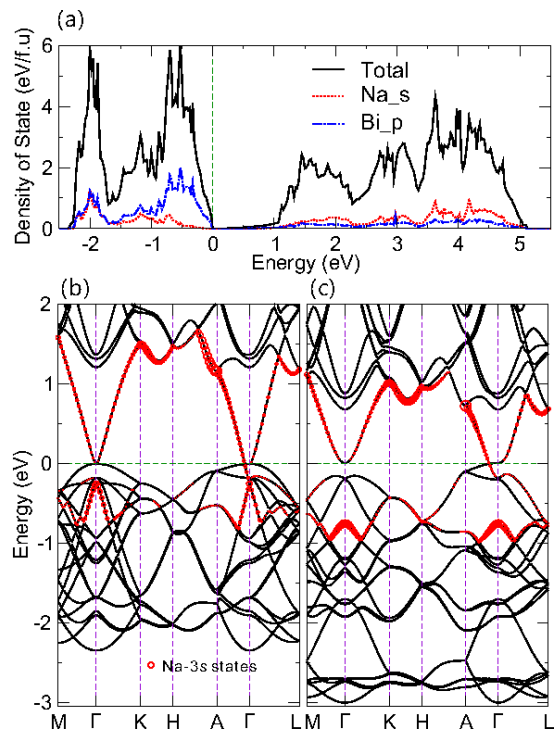


FIG. 4: The calculated electronic structures of the $P\bar{3}c1$ - Na_3Bi . (a) The total and partial density of states. (b) and (c) The band structures without and with spin-orbit coupling effects, respectively. The red circles indicate the projection to the Na-3s states.

From Fig. 1(c and i), both $P6_3/mmc$ and $P6_3cm$ phases of Na_3Bi exhibit the imaginary phonon frequencies around the K and Γ point, respectively. This fact demonstrates their structural instabilities at the ground state. From the analysis of the eigenvectors from the phonon calculation, we found two soft transverse acoustic (TA) mode on Na atoms being orthogonal to the bismuth plane. It reveals that the $P6_3/mmc$ phase can be converted into a dynamically stable structure by tuning the Na atoms along the direction of soft modes. Fortunately, these atomic vibrational directions are exactly the same orientations that the Na atoms distort to in the $P\bar{3}c1$ phase, as discussed above. As a further supporting evidence, there is no imaginary phonon frequencies in the $P\bar{3}c1$ structure (Fig. 1(f)), which indicates the dynamical stability of the $P\bar{3}c1$ structure at the ground state.

Because the valence number of the Na atom is much less than that of Bi and the Bi networks remain unchanged in the three structures, it is highly difficult to distinct them from the powder XRD patterns. As analyzed in details for LaF_3 and Na_3N ^{28,29}, their XRD patterns of both the $P\bar{3}c1$ and $P6_3cm$ structures are so close that it is impossible to distinguish these structures. Lucky, through our calculations for Na_3Bi , the candidate of the $P6_3cm$ structure can be safely excluded due to its instability of phonon dispersion at the ground state. Interestingly, we note that the simulated XRD patterns (Cu K_α , Fig. 3) for both the metastable $P6_3/mmc$ structure and the ground state $P\bar{3}c1$ one show minor differences. As illustrated

in Fig. 3, there are two additional small peaks at (022) and ($\bar{1}31$) which can be clearly seen in the $P\bar{3}c1$ phase. Therefore, we believe that the careful XRD experimental measurements can effectively distinguish these two phases.

Figure 4 further compiles the calculated electronic structure of the $P\bar{3}c1$ structure. It has been noted that its electronic structures are almost the same as what the metastable $P6_3/mmc$ structure exhibits¹. From the density of states in Fig. 4(a), the Na-3s and Bi-6p states dominates the valence and conduction bands, respectively. As evidenced in Fig. 4(b), the top valence bands are mostly occupied by the Bi-6p_{x,y} states, whereas the conduction bands comprised mostly by the Na-3s states with highly strong dispersion. In similarity with the $P6_3/mmc$ phase¹, the most crucial feature of the $P\bar{3}c1$ structure also shows an inverted band structure. In the case without the inclusion of the spin-orbit coupling (SOC) effect, the Na-3s state lies in the valence bands, being energetically lower than the Bi-6p_{x,y} states by about 0.26 eV at the Γ point. By switching on the SOC effect, the Na-3s state becomes even lower in energy by 0.75 eV than the Bi-6p_{x,y} states. Although the inverted band structure appears, the $P\bar{3}c1$ structure is not a nontrivial topological insulator. In contrast, it is a topological semimetal with two 3D bulk Dirac points at (0, 0, $k_z \approx \pm 0.256\frac{\pi}{c}$) along the Γ -A direction as shown in Fig. 4(c), being exactly the same with that of the $P6_3/mmc$ phase¹. Importantly, in similarity to the $P6_3/mmc$ phase¹ the 3D Dirac cones are indeed protected by the threefold rotation

crystal symmetry in the $P\bar{3}c1$ structure. Although in this case, the graphite-like Na/Bi sheets are buckled due to the shifting of Na2 atoms, its threefold rotation symmetry still remains unchanged. Within this condition, the 3D bulk Dirac cones would be highly robust. In addition, it needs to be mentioned that each 3D bulk Dirac cone is fourfold degenerated, linearly dispersing around the Fermi point. The appearance of the 3D bulk Dirac cones can be viewed as "3D graphene"^{1,2}.

Summarizing, in comparison with the early characterized metastable $P6_3/mmc$ phase of Na₃Bi, we found a new stable ground-state phase of the $P\bar{3}c1$ structure, which is both energetically and dynamically more stable. Interestingly, the metastable $P6_3/mmc$ phase is dynamically unstable at the ground state due to the presence of the imaginary phonon frequencies around the K point in the BZ. Importantly, our results also uncovered that the $P\bar{3}c1$ phase at the ground state is a topological 3D Dirac semimetal, exhibiting exactly same electronic states of the $P6_3/mmc$ phase.

Acknowledgements

The authors are grateful for financial supports from the "Hundred Talents Project" of the Chinese Academy of Sciences (CAS) and from the National Natural Science Foundation of China (NSFC) (No. 51074151). Calculations in China were performed in the HPC cluster at IMR.

* Corresponding author: xingqiu.chen@imr.ac.cn

- ¹ Z. Wang, Y. Sun, X.-Q. Chen, C. Franchini, G. Xu, H. Weng, X. Dai, Z. Fang, Phys. Rev. B **85**, 205101 (2012).
- ² Z. K. Liu, B. Zhou, Y. Zhang, Z. J. Wang, H. M. Weng, D. Prabhakaran, S.-K. Mo, Z. X. Shen, Z. Fang, X. Dai, Z. Hussain, and Y. L. Chen, Science **343**, 864 (2014).
- ³ S.-Y. Xu, C. Liu, S. K. Kushwaha, T.-R. Chang, J. W. Krizan, R. Sankar, C. M. Polley, J. Adell, T. Balasubramanian, K. Miyamoto, N. Alidoust, G. Bian, M. Neupane, I. Belopolski, H.-T. Jeng, C.-Y. Huang, W.-F. Tsai, H. Lin, F. C. Chou, T. Okuda, A. Bansil, R. J. Cava, and M. Z. Hasan, Preprint at <http://arXiv:1312.7624> (2013).
- ⁴ S. M. Young, S. Zaheer, J. C. Y. Teo, C. L. Kane, E. J. Mele, and A. M. Rappe, Phys. Rev. Lett. **108**, 140405 (2012).
- ⁵ A. H. Castro Neto, N. M. R. Peres, K. S. Novoselov and A. K. Geim, Rev. Mod. Phys., **81**, 109 (2009).
- ⁶ X. G. Wan, A. M. Turner, A. Vishwanath, S. Y. Savrasov, Phys. Rev. B **83**, 205101 (2011).
- ⁷ Z. Fang, N. Nagaosa, K. S. Takahashi, A. Asamitsu, R. Mathieu, T. Ogasawara, H. Yamada, M. Kawasaki, and K. Terakura, Science, **302**, 92-95 (2003).
- ⁸ G. B. Halasz and L. Balents, Phys. Rev. B, **85**, 035103 (2012).
- ⁹ S. Murakami, New J. Phys. **9**, 356 (2007).
- ¹⁰ Z. Wang, H. Weng, Q. Wu, X. Dai, and Z. Fang, Phys. Rev. B, **88**, 125427 (2013).
- ¹¹ K.-Y. Yang, Y.-M. Lu, Y. Ran, Phys. Rev. B **84**, 075129 (2011).
- ¹² M. Orlita, D. M. Basko, M. S. Zholudev, F. Tepe, W. Knap, V. I. Gavrilenko, N. N. Mikhailov, S. A. Dvoretiskii, P. Neugebauer, C. Faugeras, Nature Phys. **10**, 233 (2014).
- ¹³ M. N. Chernodub, A. Cortijo, A. G. Grushin, K. Landsteiner, M. A. H. Vozediano, Phys. Rev. B, **89**, 081407 (2014).
- ¹⁴ E. V. Gorbar, V. A. Miransky, I. A. Shovkovy, Phys. Rev. B, **89**, 085126 (2014).
- ¹⁵ Y. Qminato, M. Koshino, Phys. Rev. B, **89**, 054202 (2014).
- ¹⁶ S. M. Young, S. Chowdhury, E. J. Walter, E. J. Mele, C. L. Kane, and A. M. Rappe, Phys. Rev. B **84**, 085106 (2011).
- ¹⁷ M. Neupane, S. Yang Xu, N. Alidoust, G. Bian, C. Liu, I. Belopolski, T. -R. Chang, H.-T. Jeng, H. Lin, A. Bansil, F. C. Chou, M. Z. Hasan, Preprint at <http://arXiv:1309.7892> (2013).
- ¹⁸ S. Borisenko, Q. Gibson, D. Evtushinsky, V. Zabolotnyy, B. Buechner, R. J. Cava, Preprint at <http://arXiv:1309.7978> (2013).
- ¹⁹ G. Brauer, Zintl. E., Z. Phys. Chem. Abstr. **37**, 323 (1937).
- ²⁰ M. Mansmann, Z. Kristallogr., **122**, 399 (1965).
- ²¹ P. Hafner and K. -J. Range, J. Alloys Compd. **216**, 7 (1994).
- ²² K. J. Range, R. Ehrl, and P. Hafner, J. Alloys Compd. **240**, 19 (1996).
- ²³ K.-J. Range and P. Hafner, J. Alloys Comp. **183**, 430 (1992).
- ²⁴ K.-J. Range and P. Hafner, J. Alloys Comp. **191**, L5 (1993).
- ²⁵ O. Olofsson, Acta Chem. Scand. **26**, 2777 (1972).
- ²⁶ H. Kerber, H. -J. Deiseroth, and R. Walther, Z. Kristallogr. New Cryst Struct. **213**, 473 (1998).
- ²⁷ H. Hirt and H. J. Deiseroth, Z. Kristallogr. NCS **218**, 6 (2003).
- ²⁸ G. Vajenine, X. Wang, I. Efthimiopoulos, S. Karmakar, K. Syassen, and M. Hanfland, Phys. Rev. B **79** (22) (2009).
- ²⁹ W. A. Crichton, P. Bouvier, B. Winkler, and A. Grzechnik, Dalton Trans. **39** (18), 4302 (2010).
- ³⁰ P. Villars and L. D. Calvert, *Pearson's Handbook of Crystallographic Data for Intermetallic Phase*, (American Society for Met-

- als, Metals Park OH 1985).
- ³¹ H. J. Beister, S. Haag, R. Kniep, *Angew. Chem.*, **100**, 1116 (1988).
- ³² S. Takeda, S. Tamaki, *J.Phys.:Condens.Matter*, **2**, 10173 (1990).
- ³³ H. J. Beister, J. Klein, I. Schewe, K. Syassen, *Hig. Pres. Res.* **7**, 91 (1991).
- ³⁴ J. Sangster, A.D. Pelton, *J. Phase Equil.* **12** 451 (1991).
- ³⁵ M. Tegze and J. Hafner, *J.Phys.:Condens.Matter*, **4**, 2449 (1992).
- ³⁶ M. E. Leonova, S. A. Kulinich, and L. G. Sevast'yanova, *et al.*, *Exp. Geosci.* **7**, 55 (1998).
- ³⁷ S. A. Kulinich, M. E. Leonova, and L. G. Sevast'yanova, *et al.*, *Zh. Obshch. Khim.* **69**, 681 (1999).
- ³⁸ M.E. Leonova, I. K. Bdikin, S.A. Kulinich, O.K. Gulish, L.G. Sevast'yanova, K.P. Burdina, *Inorg. Mater.* **39**, 266-270 (2003).
- ³⁹ P. Hohenberg, *Phys. Rev. B* **136**, 864 (1964).
- ⁴⁰ W. Kohn and L. J. Sham, *Phys. Rev. A* **140**, 1133 (1965).
- ⁴¹ G. Kresse and J. Hafner, *Phys. Rev. B* **47**, 558 (1993).
- ⁴² G. Kresse and J. Furthmüller, *Phys. Rev. B* **54**, (11169) 1996.
- ⁴³ P. E. Blöchl, *Phys. Rev. B* **50**, 17953 (1994).
- ⁴⁴ J. P. Perdew, K. Burke, and M. Ernzerhof, *Phys. Rev. Lett.* **77**, 3865 (1996).
- ⁴⁵ A. Togo, F. Oba, I. Tanaka, *Phys. Rev. B* **78**, 134106, 2008.